J. Inst. Eng. India Ser. D (July–December 2023) 104(2):723–738
https://doi.org/10.1007/s40033-022-00412-3

ORIGINAL CONTRIBUTION

Optimization of Wear Parameters on Friction Stir Welded Dissimilar Aluminium Joints

M. Madhusudan[1] · S. P. Shanmuganatan[1] · Shridhar Kurse[2]

Received: 31 March 2022 / Accepted: 15 September 2022 / Published online: 10 October 2022

Abstract The welds in this study were prepared by adapting a two-pass friction stir welding strategy with a cylindrical pin tool rotated and traversed at 800 RPM and 40 mm/min, respectively. Four pins of parent alloys (AA 6061 and AA 7075), unreinforced, and reinforced weld were subjected to wear characteristic testing. The experimental trials were performed as per Taguchi L_{16} orthogonal array using a pin-on-disc machine with varied input parameters like plate/pin type, applied load, sliding velocity, and sliding distance. The output responses namely the wear rate, wear resistance, and coefficient of friction for different pins were analysed using the MINITAB tool, and wear parameters were optimized. The main effects plot presented a reinforced weld pin, an applied load of 10 N, a sliding velocity of 1 m/s, and a sliding distance of 2000 m as optimal conditions for better wear responses. This could be due to the presence of the h-BN phase in dissimilar weld matrix contributing to the emergence of tribo-layer at the interface, dynamic surface interaction, and high dislocation density. Individual response optimization and grey relational analysis are found to be reasonably matched. A confirmation test was performed using the best parameter combination, and the results were compared.

Keywords Two pass FSW · Nano composite · Wear parameters · ANOVA · Grey relational analysis

✉ M. Madhusudan
kashyapa.madhu@gmail.com

[1] Department of Mechanical Engineering, Dayananda Sagar College of Engineering, Bengaluru 560078, India

[2] Department of Automobile Engineering, New Horizon College of Engineering, Bengaluru 560103, India

Introduction

The friction Stir Welding (FSW) technique offers advantages over fusion welding with respect to reduction in fumes, porosity, and distortion. A non-consumable tool is rotated at high speed over the substrate and generates stirring action during the process to produce a firm weld. Light weight alloys especially Aluminium Alloys (AA 6061 and AA 7075) exhibit excellent mechanical properties with good weldability and corrosion resistance. These alloys find considerable usage in stir welding techniques occupying suitable applications in the fuselage, panels, and structures of aircraft. Reinforcing particle like hard boron nitride demonstrates superior tribological properties, high load-bearing properties, excellent lubricity, and decomposition resistance. Fabricated Aluminium Matrix Composites (AMCs) serve structural and tribological features like pistons, connecting rods, timing gears, and crankcases in automobile sectors.

Singh et al. [1] produced similar and dissimilar joints via FSW to study their mechanical and microstructural characteristics. The study concluded that the average microhardness for dissimilar welds is comparatively higher as compared to similar ones. Surrya Prakash et al. [2] studied the tribological and mechanical properties of AA 6061-based hybrid composites produced by a sintering process. TiB_2 reinforced hybrid composites with 4 and 6 wt. % showed reduced order of wear rate with enhanced hardness. Fine matrix and reinforcement bonding also exhibited high friction coefficient.

Paidpilli et al. [3] observed the microstructure and wear characteristics of AA 6061 obtained through mixing and ball milling. The wear test conducted at varying loads (10–40 N) resulted in enhanced wear characteristics and at higher loads, tribo-layer was sustained by ball milled aluminium-5 vol% lead alloy. Kumar et al. [4] compared the

wear characteristics of AA 6351 in-situ composites reinforced with ZrB_2 in dry sliding conditions under the cast, solutionized, and aged environmental conditions. The reduction in wear rate was reported for the solutionized and aged samples. Moreover, the frictional coefficient appears to be high for as-cast samples.

Kasirajan et al. [5] observed the influence of welding parameters on the strength and tribological features of stir welded AA 5052-AA 6101 T6 using L_{16} orthogonal array. The observations stated that the combined effect of offset distance (1 mm) and spindle speed 1400 rpm results in improved said properties as compared to tool offset of 2 mm and 765 rpm. Kumar et al. [6] evaluated the strength characteristics of stir welded AA 6101 T6-AA 1350 taking into account the influence of the tool pin. It is noticeable from the study that compared to triangular and circular pins, the joint fabricated using hexagonal geometry yielded better tensile strength.

Kannan et al. [7] investigated the wear behaviour of squeeze cast AA 7075 hybrid composites using Response Surface Methodology (RSM). The hybrid nanocomposite exhibited improvement in wear resistance and friction coefficient of the order 63% and 18.5%, respectively. Samal et al. [8] assessed the sliding wear characteristics of AA 5052-TiC reinforcement fabricated by stir casting technique using multi-response optimization. The optimized results were compared with the findings of the fuzzy logic system. The observed percentage deviation for fuzzy logic and the earlier is less than 10, highlighting the potentiality of the fuzzy system in evaluating the wear behaviour of the composites.

Dinaharan et al. [9] predicted the wear rate of friction stir processed copper composites reinforced with SiC, TiC, Al_2O_3, WC, and B_4C using an artificial neural network. The authors observed the lower order of wear rate with B_4C reinforced composites. Ikumapayi et al. [10] demonstrated the mechanical and tribological properties of AMC fabricated via Friction Stir Processing (FSP) technique. The applied load of 50 N revealed a significant improvement in the wear properties.

Naik et al. [11] fabricated the copper surface composites by reinforcing tungsten particles and optimized the stir processing parameters using the Taguchi L_9 technique. The yielding of maximum wear resistance with the inclusion of 10 vol% of tungsten particles is reported. Girish et al. [12] conducted wear studies on stir-processed 7075 aluminium alloy in dry sliding conditions and developed a regression model to evaluate wear rate. The optimal values for load, sliding velocity, and sliding distance were found to be 9.81 N, 2 m/s, and 2000 m, respectively.

Adediran et al. [13] conducted the wear performance test on aluminium reinforced with silicon-based compounds and inferred that the increase in the applied load results in the reduction of friction coefficient significantly. The study also revealed that the initial wear mechanism was adhesive and later abrasive. Saravanakumar et al. [14] employed Taguchi and generalized regression neural network to study the parametric influence on wear responses of AA 2219-graphite composite. Compared to the linear regression model, the regression neural network exhibits a better output by reducing experimental cost and testing time.

Zhao et al. [15] utilized the hot-press sintering method to produce 5083 aluminium matrix composite with B_4C as reinforcement. The study disclosed that with the increase in B_4C content, there is a diminishing wear loss with the uptrend in friction coefficient. Coyal et al. [16] studied the mechanical and wear characteristics of AMC and in their study, the composite fabricated via stir casting showcased fourfold improved resistance to wear in contrast to the parent.

Mata et al. [17] analysed the wear resistance property of friction stir welded A359 reinforced with SiC. Wear parameters of three welded joints were analysed and compared with the parent. The experimentation concluded that all the welded joints exhibited low frictional coefficient and discrete microstructural refinement resulted in reduced order of wear resistance on the welding segment.

It is observed from the previous literature that sufficient studies optimizing the wear characteristics of AMCs reinforced with SiC, B_4C produced via stir casting (liquid metallurgy), ball milling, pressing, and stir processing techniques exist. However, the findings related to optimization of wear parameters on friction stir unreinforced, nanocomposite (h-BN reinforced) dissimilar welds performed with two pass and parent alloys (AA 6061 T6 and AA 7075 T651) are limited. Hence, the present study addresses the performance evaluation of wear parameters using individual response and multi-objective optimization methods.

Materials and Methods

Commercially available ingot plates, AA 7075 T651 and AA 6061 T6 (supplier: PMC Corporation, INDIA) of dimension $150 \times 100 \times 6.5$ mm were chosen as the parent material. 5 vol% of h-BN (hexagonal Boron Nitride) powder of 99% purity having 50 nm average particle size (supplier: ULTRA-NANOTECH. Pvt. Ltd) was used as the reinforcing material to produce dissimilar nanocomposite weld.

The fabrication route chosen to obtain the weld is FSW, a solid-state joining process wherein the generation of heat is accelerated by friction at the tool-work interface. With the softening of the metal, the plasticized material is transferred from the front end to the rear edge and forged with high pressure by the firm contact of the tool shoulder to produce a sound weld between the work pieces.

Cylindrical pin tool (made of M-42 high-speed steel) possessing increased surface contact rotating at 800 rpm and 40 mm/min feed establishes enhanced tensile strength and joint efficiency. Two-pass FSW aids in ultra-grain refinement and uniform distribution of nanoparticles [18]. Consequently, a tool with cylindrical pin geometry at 40 mm/min and 800 rpm spindle speed involving two pass welding was the operating level for preparing both unreinforced and reinforced welds. 8 mm diameter pins, four in numbers were extracted from both parent alloys (AA 6061 and AA 7075), unreinforced and reinforced weld. Wear studies were carried out on pin-on-disc following ASTM G99 standards [19]. The experimental setup and the extracted pins for the study are shown in Fig. 1a, b.

Weld pins extracted were held in position using backup mild steel pins. Steel disc of material EN-31 grade is rotated contacting the pin for 30–40 min. The test was carried out for varied sliding velocity, normal load, and sliding distance under the ambient condition with the application of normal load on each specimen contacting the disc. After every test the specimen was removed, cleaned with acetone, dried, and weighed to calculate the weight loss thereby wear rate, wear resistance, and Coefficient of Friction (COF) were determined. The wear input parameters and their levels are displayed in Table 1. Based on multiple wear parameters and output responses, the input levels for the wear parameters were designed as per the L_{16} orthogonal array (four factors and four levels design). Table 2 indicates a statistical chart for input variables.

ANOVA (Analysis of Variance) and Grey relational analysis were employed to study the influence of each wear parameter on individual and combined responses. 'Smaller

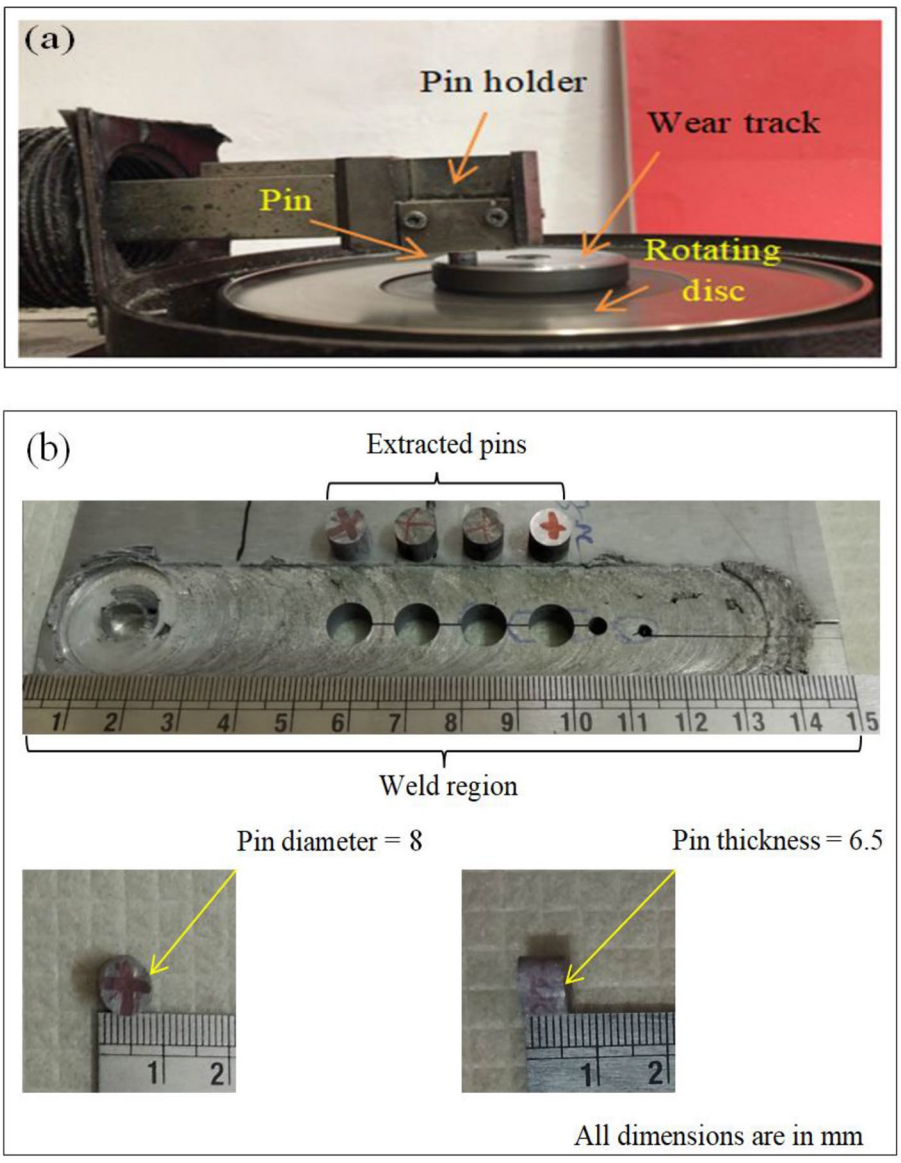

Fig. 1 **a** Wear test, **b** Extracted pins

Table 1 Statistical input table for independent variables

Sl. no	Wear parameters	Levels			
		1	2	3	4
1	Plate/pin type (*P*)	AA 6061	AA 7075	Unreinforced	Reinforced
2	Applied load (*L*) in N	10	15	20	25
3	Sliding velocity (*V*) in m/s	0.6	0.8	1.0	1.2
4	Sliding distance (*D*) in m	500	1000	1500	2000

Table 2 Statistical L_{16} orthogonal array table

Runs	*P*	*L*	*V*	*D*
1	1	1	1	1
2	1	2	2	2
3	1	3	3	3
4	1	4	4	4
5	2	2	1	3
6	2	1	2	4
7	2	4	3	1
8	2	3	4	2
9	3	3	1	4
10	3	4	2	3
11	3	1	3	2
12	3	2	4	1
13	4	4	1	2
14	4	3	2	1
15	4	2	3	4
16	4	1	4	3

the better' and 'Larger the better' concepts were implemented in the present study for Signal-to-Noise (S/N) ratio calculation and grey relational normalization. Equations calculating the S/N ratio are represented below:

$$\text{Smaller the better:} \quad \frac{S}{N} = -10\log\left\{ {}^{1}\!/_{n} \sum_{i=1}^{n} y_i^2 \right\} \tag{1}$$

$$\text{Larger the better:} \quad \frac{S}{N} = -10\log\left\{ {}^{1}\!/_{n} \sum_{i=1}^{n} 1 \Big/ y_i^2 \right\} \tag{2}$$

The following are the equations for grey relational normalization:

$$\text{Smaller the better:} \quad x_i^*(k) = \frac{\max x_i^0(k) - x_i^0(k)}{\max x_i^0(k) - \min x_i^0(k)} \tag{3}$$

$$\text{Larger the better:} \quad x_i^*(k) = \frac{x_i^0(k) - \min x_i^0(k)}{\max x_i^0(k) - \min x_i^0(k)} \tag{4}$$

where $x_i^*(k)$ and $x_i^0(k)$ indicates reference and original sequence.

Grey relational coefficient is determined by the following equation:

$$\zeta_i^*(k) = \frac{\Delta_{\min} + \zeta * \Delta_{\max}}{\Delta_{0i}(k) + \zeta * \Delta_{\max}} \tag{5}$$

where $\zeta_i^*(k)$ is Grey relational co-efficient, $\Delta_{\min}$ and $\Delta_{\max}$ are minimum and maximum deviations. 'ζ' is said to be distinguishing coefficient whose value is 0.5.

Grey Relational Grade (GRG) is calculated by considering the average of grey relational coefficient of each response.

Results and Discussion

Wear test results are consolidated using MINITAB 20.1 software tool. The empirical and statistical methods are employed for modelling and analysis of output responses. The objective of the study is to optimize the wear process parameters. The parameters were evaluated for significance at a 95% confidence level. Table 3 shows the analytical responses for input factors such as plate/pin type, sliding distance, sliding velocity, and applied load. Trial runs were analysed through ANOVA to establish a regression model between wear responses and the parameters.

Based on the experimental output responses, regression equations were developed to correlate input and output variables. The regression equation/model representing the wear rate, wear resistance, and COF is given by the following relation:

$$\begin{aligned}\text{Wear rate} =& 0.523 - (0.2600 * P) + (0.08900 * L) \\ & - (0.075 * V) - (0.000030 * D)\end{aligned} \tag{6}$$

$$\begin{aligned}\text{Wear resistance} =& 0.585 + (0.2845 * P) - (0.07180 * L) \\ & + (0.785 * V) + (0.000188 * D)\end{aligned} \tag{7}$$

$$\begin{aligned}\text{COF} =& 0.1294 + (0.03275 * P) - (0.00005 * L) \\ & - (0.0088 * V) + (0.000117 * D)\end{aligned} \tag{8}$$

$$\begin{aligned}\text{GRG} =& 0.3109 + (0.0779 * P) - (0.0788 * L) \\ & + (0.0305 * V) + (0.0525 * D)\end{aligned} \tag{9}$$

Table 3 Analytical response table for input variables

Runs	S/N ratios			Mean		
	Wear rate (mg m/min)	Wear resistance	COF	Wear rate (mg m/min)	Wear resistance	COF
1	− 1.58362	− 1.51441	− 13.9794	1.2	0.84	0.20
2	− 3.52183	− 3.47850	− 11.7005	1.5	0.67	0.26
3	− 4.60898	− 4.58296	− 9.6297	1.7	0.59	0.33
4	− 7.95880	− 7.95880	− 9.1186	2.5	0.40	0.35
5	− 0.82785	− 0.81917	− 8.1787	1.1	0.91	0.39
6	0.91515	0.98436	− 6.9357	0.9	1.12	0.45
7	− 6.84845	− 6.74484	− 10.4576	2.2	0.46	0.30
8	− 3.52183	− 3.47850	− 9.6297	1.5	0.67	0.33
9	− 2.27887	− 2.27019	− 7.3306	1.3	0.77	0.43
10	− 6.44439	− 6.37518	− 8.6360	2.1	0.48	0.37
11	4.43697	4.45433	− 10.1728	0.6	1.67	0.31
12	0.91515	0.98436	− 12.7654	0.9	1.12	0.23
13	− 4.60898	− 4.58296	− 9.1186	1.7	0.59	0.35
14	− 0.82785	− 0.81917	− 9.6297	1.1	0.91	0.33
15	6.02060	6.02060	− 5.6799	0.5	2.00	0.52
16	7.95880	7.95880	− 7.5350	0.4	2.50	0.42

The normal probability plots used for assessing the data for wear rate, wear resistance and COF are shown in Fig. 2a–c. The centre, upper and lower line on the plot indicates that the percent of points fall at a given level of wear responses within a 95% confidence interval.

The goodness-of-fit in regression and ANOVA is examined by the residual plot. It is observed from Fig. 3a–c that the residuals (errors) are normally distributed along a straight line. Wear response value lies on or between − 2 and + 2 indicating that a regular pattern is observed in the model. From the residuals versus fitted value plot, residuals are randomly scattered conforming appropriate linear model. The histogram of the residuals follows a fair normal distribution. The residuals versus order plot highlight that the residuals fall around the centre line indicating a good correlation [20].

The regression models developed were validated using ANOVA and the results are presented in Tables 4, 5 and 6. The determination coefficient (R^2) indicates appropriate models. In the present study, the value of the determination coefficient (R^2) for the wear responses is around 95% signifying the model. Predicted and adjusted R^2 are in fair agreement. The probability value is lesser than 'F' highlighting that the model is significant [21]. The predicted and experimental response fits well.

From the analysis, the model obtained is adequate for the prediction of wear responses. It was inferred that for the observation of wear rate and wear resistance, the influence of load is superior compared to other input variables. Considering COF, the influence of sliding distance overcomes the other parameters.

In the initial stage, the wear process is adhesive wherein the pull out of the fragments from the surface of the worn pin to the disc takes place. Particle adherence to the disc surface leads to abrasion-inducing crest and trough in due course. After a few seconds, the strategy of three body wear progresses into action thereby the interaction between abrasive particle and counter body proceeds with the commencement of perforations leading to excessive material loss. Under a sliding wear environment, worn out of particles adjoining aluminium matrix takes place. The reinforcement particles are exposed and later, contact the steel counter face. The wear rate gets reduced once the particles are projected.

The interaction and contour plots for different process attributes on wear rate, wear resistance, and COF are discussed in Figs. 4, 5, and 6. From Fig. 4a, the plot of applied load on wear rate for different plate/pin types indicate that wear rate steps up gradually as the load pronounces from 10 to 25 N. The parallel lines indicate there is no interaction between the input and output parameters. The lower wear rate identified at lower load is indicated by the light green region and is represented in Fig. 4b. Dominant dark green distribution highlights the higher order of wear rate as shown in Fig. 4c. The occurrence of this region in the graph evidence that the reinforced weldment (h-BN reinforced) possess the lowest wear rate compared to the unreinforced and parent.

Referring to Fig. 4a plot on sliding velocity versus wear rate for different pin types, the non-parallel lines indicate that there is an interaction. As velocity ascends from 0.6 to 1.2 m/s, an increase in wear rate is observed. The reinforced pin type showcased lower order of wear rate

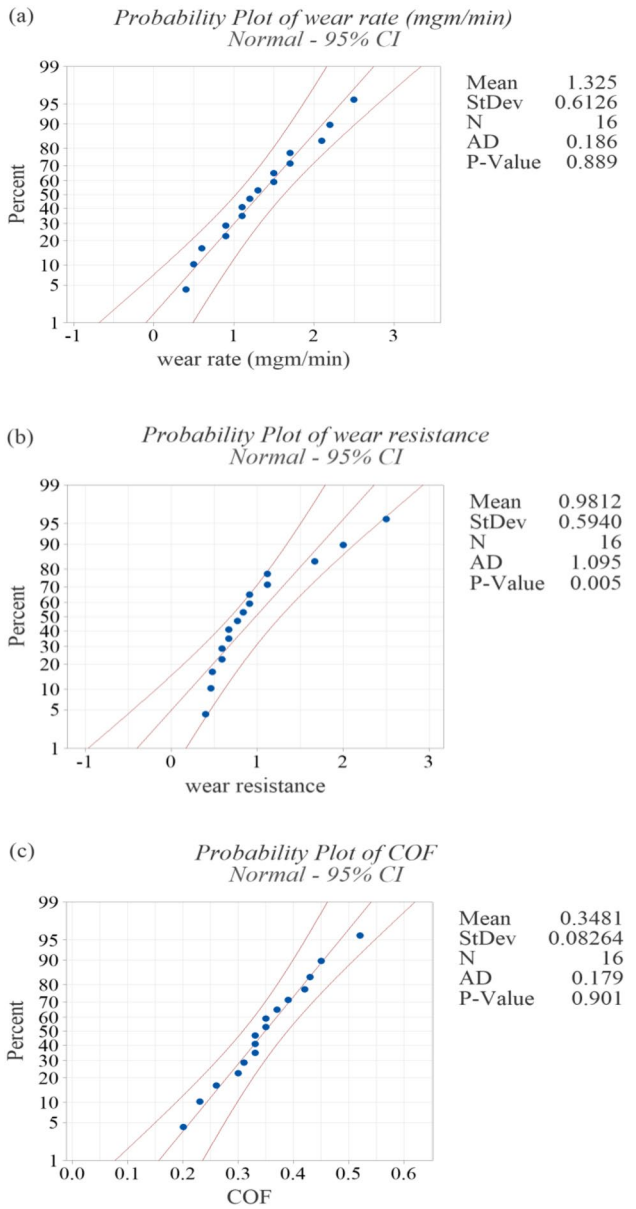

Fig. 2 Normal probability plot for; **a** wear rate, **b** wear resistance, and **c** COF

(0.5–1 mg m/min). At the same time wear rate exhibited by unreinforced weld and parent material is high. The presence of a light green region (a portion of sliding velocity from 1.0 to 1.2 m/s) exhibits the lowest wear rate in contrast to other pins. The results from the analysis showcased that the wear rate experienced by reinforced pin (AA 6061 + AA 7075 + h-BN) is low and is in good agreement with previous research [22].

Referring to the plot on distance versus wear rate for different pin types, the wear rate exhibited by the reinforced pin is less in comparison with others. Velocity versus wear rate plot for different applied loads showed the decreasing trend of wear rate at 10 N. A similar trend is also noticeable in Fig. 4a plot of sliding distance versus wear rate for the varied load. Figure 4a also represents sliding distance versus wear rate for varied velocity and is indicative of lower order of wear rate at 1.0 m/s. Figure 4d indicates the variation in wear rate concerning sliding distance for different pins. At 2000 m distance, reinforced pin rendered reduced order of wear rate.

The reinforcement, h-BN possesses good lubricity and high fracture toughness by nature. Transfer of load between the reinforcement particle and the weld results in effective cohesion imparting enhanced wear resistance.

Figure 5a–d illustrates the interaction effect of process parameters on wear resistance. Figure 5a shows the interaction of pin type on applied load indicates the higher wear resistance at a load of 10 N. Figure 5b exhibited maximum wear resistance value ranging from 2.0 to 2.5 for the composite pin. It is evidenced from Fig. 5c that wear resistance pronounces as sliding velocity peaks up both for the unreinforced and reinforced pin. Subsequently, 1500–2000 m sliding distance and composite pin interaction were significant for higher wear resistance (dark green region) as indicated in Fig. 5d.

The friction prevailing at the contact surface is measured in terms of COF. Sliding generates friction between contacting surfaces which aids in temperature rise. Friction originates from the surface chemistry over the wearied portion. The occurrence of frictional coefficient with sliding velocity could be associated with the effectual surface reciprocity as influenced by interface temperature. The condition of mild and moderate oxidative zone prevails during the process. Thermal gradient results in shifting of the zone thereby higher frictional values. The reduction in frictional coefficient is due to the tribo chemical event and simultaneous formation of tribo film functioning as a protective layer between the mating surfaces [23].

The interactive influence of process attributes on COF is illustrated in Fig. 6a–d. On inferring the graph, parallel lines showed nil interaction and non-parallel lines indicate the interaction of significance. Referring to Fig. 6a, it is noticeable that the interaction of pin type with increasing values of sliding distance is significant for a reinforced pin. It is observed from Fig. 6b that the COF value for a reinforced pin is maximum at load varied from 10 to 15 N. Considering the 1.0 m/s sliding velocity, a COF value exhibited by the reinforced pin varied from 0.45 to 0.5 and is indicated in Fig. 6c. Eventually, the composite pin showed increased order of COF at 2000 m sliding distance (dark green region) and is noticed from Fig. 6d. Decrease in friction coefficient could also be related with the two pass strategy incorporated in the process [24].

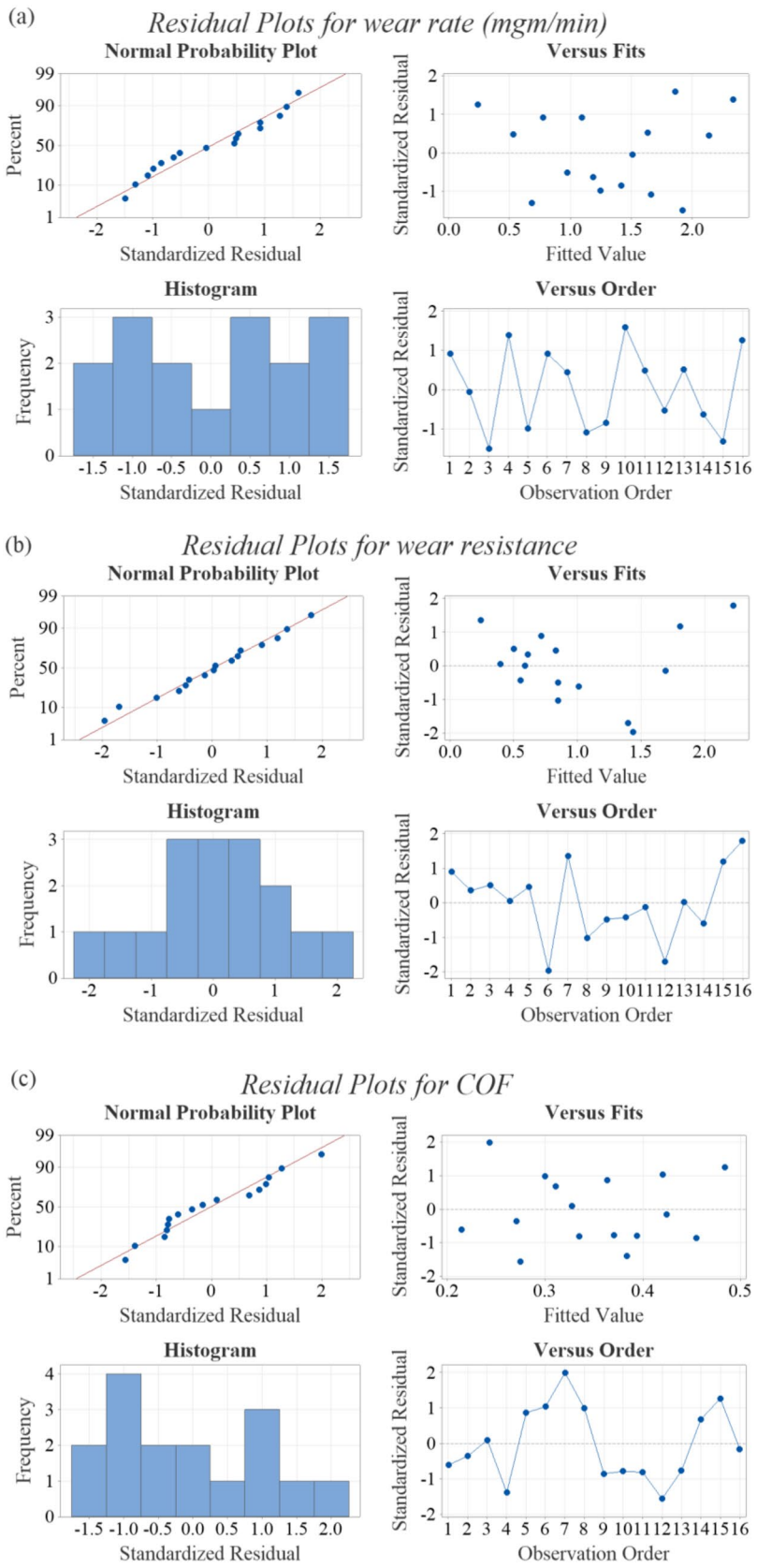

Fig. 3 Residual plots for; **a** wear rate, **b** wear resistance, and **c** COF

Table 4 ANOVA table for wear rate

Source	DF	Adj SS	Adj MS	*F* value	*P* value	% contribution
Plate/pin type	3	1.36000	0.45333	272.00	0.000	24.15
Applied load (N)	3	4.21500	1.40500	843.00	0.000	74.86
Sliding velocity (m/s)	3	0.04500	0.01500	9.00	0.052	0.799
Sliding distance (m)	3	0.00500	0.00167	1.00	0.500	0.088
Error	3	0.00500	0.00167			
Total	15	5.63000				

Table 5 ANOVA table for wear resistance

Source	DF	Adj SS	Adj MS	*F* value	*P* value	% contribution
Plate/pin type	3	1.7337	0.57789	14.27	0.028	32.755
Applied load (N)	3	2.6032	0.86774	21.42	0.016	49.183
Sliding velocity (m/s)	3	0.6091	0.20304	5.01	0.109	11.508
Sliding distance (m)	3	0.2252	0.07507	1.85	0.312	4.25
Error	3	0.1215	0.04051			
Total	15	5.2928				

Table 6 ANOVA table for COF

Source	DF	Adj SS	Adj MS	*F* value	*P* value	% contribution
Plate/pin type	3	0.031069	0.010356	54.63	0.004	30.327
Applied load (N)	3	0.000369	0.000123	0.65	0.635	0.360
Sliding velocity (m/s)	3	0.002319	0.000773	4.08	0.139	2.263
Sliding distance (m)	3	0.068119	0.022706	119.77	0.001	66.493
Error	3	0.000569	0.000190			
Total	15	0.102444				

Optimization of Wear Parameters

Empirical Modelling of wear parameters for parent alloys, unreinforced and reinforced pin have been carried out. The experimentation is designed with four factors and four levels as per Taguchi L_{16} orthogonal design [25]. "Smaller is better" and "Larger is better" concepts are employed in analysis to consider the optimal values for the pins with the lower wear rate and higher order of wear resistance and COF. The analyses based on the 'Signal to Noise' (S/N) ratio and means signify the influence of independent attributes on dependent wear responses. Based on the output responses, ranking for independent attributes is represented in Tables 7, 8, and 9.

The influential factors based on the ranking for wear rate and wear resistance are applied load, plate/pin type, sliding velocity, and distance. On the other hand, sliding distance, plate/pin type, sliding velocity, and load influence the COF to a larger extent. Following the "smaller the better" and "larger the better" approach, the optimal conditions for wear rate and wear resistance are composite pin (Plate/pin type-4), 1.0 m/s sliding velocity, 10 N load, and 2000 m sliding distance. Based on the "larger the better" concept for COF, Pin (Plate/pin type-4), the velocity of 1.0 m/s, a load of 20 N, and a distance of 2000 m are the optimal conditions arrived at. The optimal conditions for wear rate, wear resistance, and COF are shown in the main effects plot and are indicated in Fig. 7a–d.

Figure 8a–c highlights the coherent match between the predicted and actual values for wear responses. The values for each schema signify that generated empirical models are reliable to conduct prediction at a 95% confidence level.

Multi-objective Optimization using Grey relational Analysis (GRA)

In the analysis, multi-objective optimization is carried out by combining the wear output responses. The analysis involves three stages of normalizing with deviation sequence, grey relational coefficient, and grey relational grade. For normalizing calculation, the 'Smaller the better' concept is employed for wear rate, and 'Larger the better' for wear resistance and COF. Grey relational coefficients were calculated for all responses under each trial run. The normalized values, grey relational coefficient, and grey relational grade calculated for each trial run are shown in Table 10. For

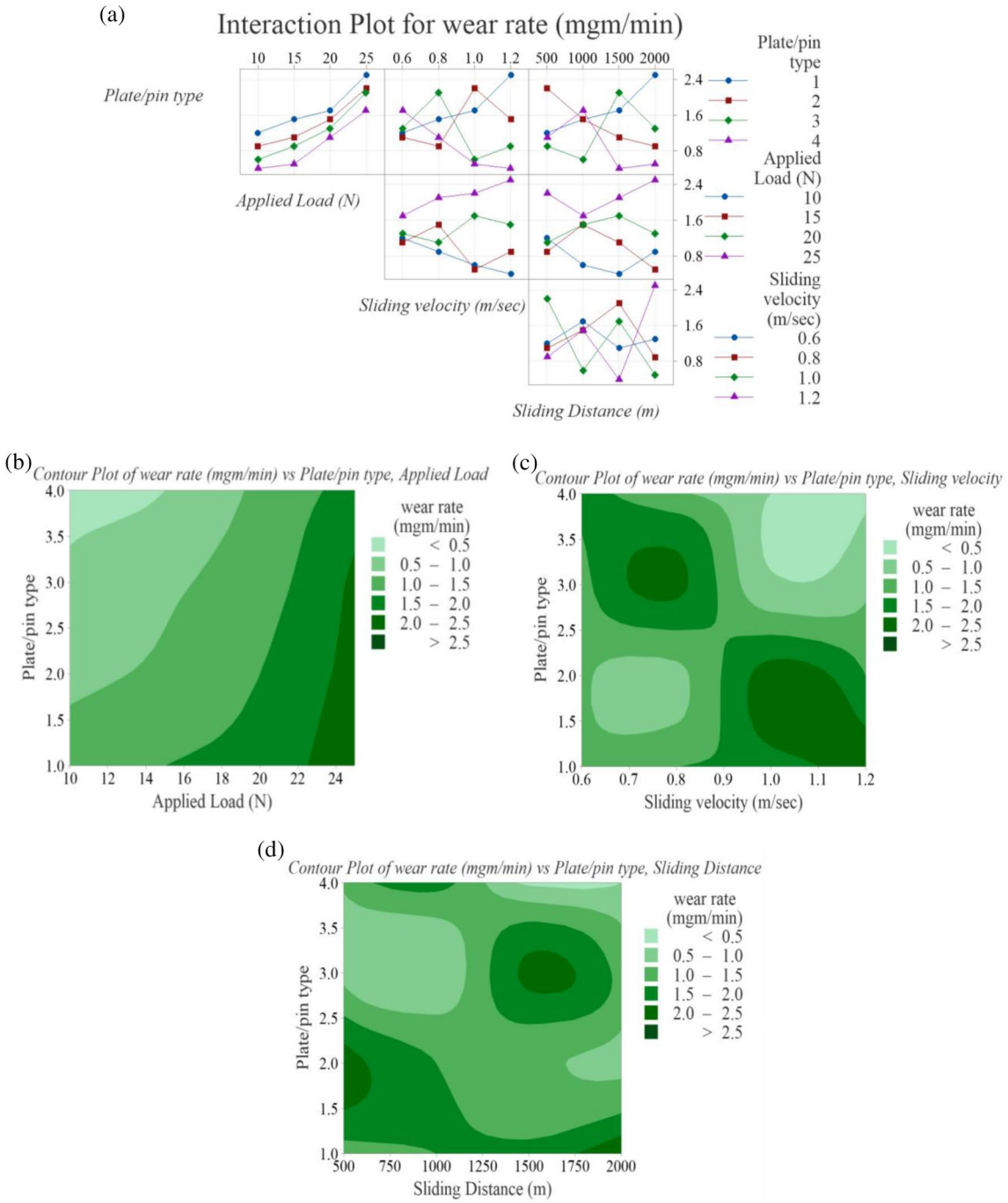

Fig. 4 **a** Interaction plot, Variations in wear rate with respect to; **b** Plate/pin type and applied load, **c** Plate/pin type and sliding velocity, and **d** Plate/pin type and sliding distance

the observation of GRG, the influence of plate/pin type is dominant as compared to other independent input variables and it is noticeable in Table 11.

In the GRA technique, promising performance is established with a maximum value of GRG. The Mean for GRG is computed based on the 'Larger the better' approach [26]. Table 12 enlist the factors influencing the grey relational grade. According to the results highlighted, Level-4 (pin type), Level-1 (Applied load), Level-3 (Sliding velocity) and Level-4 (Sliding distance) are the optimum attributes.

Figure 9 highlights the main effects plot for GRG. A higher value of GRG displayed improved performance. It was inferred that the S/N ratio shoots up while varying the plate/pin type. On the other hand, the S/N ratio showed a

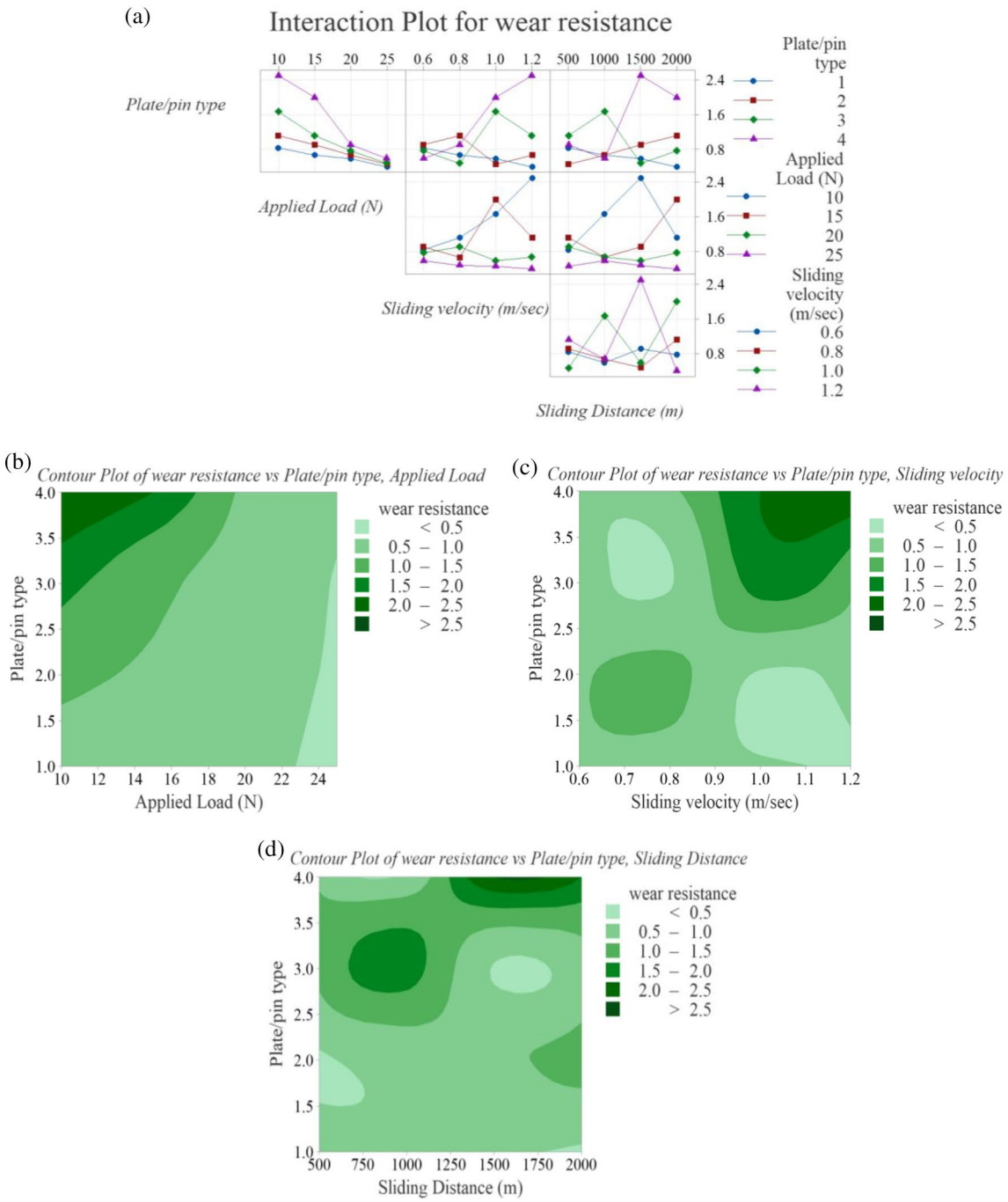

Fig. 5 **a** Interaction plot, Variations in wear resistance with respect to; **b** Plate/pin type and applied load, **c** Plate/pin type and sliding velocity, and **d** Plate/pin type and sliding distance

decrement with increased load. At the same time, the S/N ratio showed up a marginal variation with a rise in sliding velocity. For sliding distance, the S/N ratio presents a subsiding value between 500 and 2000 m. It was inferred that the optimal conditions to ensure foremost wear performance were type 4-pin, 1 m/s sliding velocity, 10 N load, and sliding distance of 2000 m.

Predicted and actual GRG shown in Fig. 10 are in fair agreement and the error variation is within 10%.

Summarily considering multi-objective optimization into the account, better wear responses are achievable for h-BN reinforced composite weld pin. This could be attributable to the properties of the base material and reinforcing

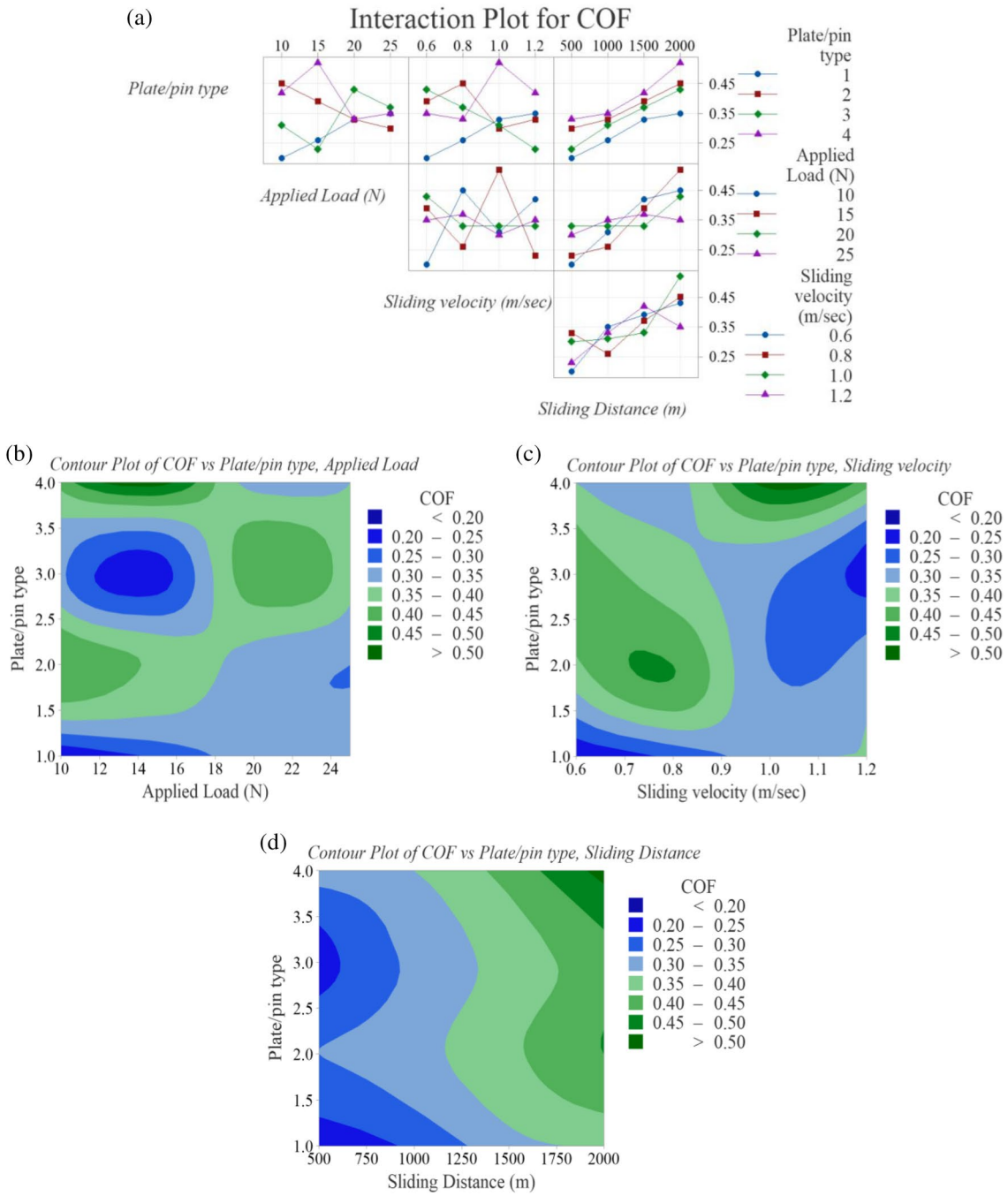

Fig. 6 **a** Interaction plot, variations in COF with respect to; **b** plate/pin type and applied load, **c** plate/pin type and sliding velocity, and **d** plate/pin type and sliding distance

nanoparticle. Besides, two-pass welding results in homogenous distribution of reinforcement in the weld region.

Furthermore, optimal load of 10 N resulted in abrasive mechanism prevailing with higher order of wear resistance attributable to the emergence of tribo-layer at the interface, lubricating nature of reinforcing particle and pronunciation of strong interfacial reinforcement bonding in the weld matrix [22]. With the optimal load of 20 N, nominal decrement in COF is observed to a certain limit due to increase in frictional force along with the increased contact surface and self-lubrication of h-BN for composite weld pin [27]. The optimal velocity of 1 m/s manifested better wear results contributing to increased interfacial temperature due to an insufficient time interval for the frictional heat transport (dynamic surface interaction). Eventually, 2000 m sliding distance showed enhanced wear outcomes by virtue

Table 7 Response table for S/N ratios of wear rate

Level	Plate/pin type	Applied load (N)	Sliding velocity (m/s)	Sliding distance (m)
1	−4.4183	2.9318	−2.3248	−2.0862
2	−2.5707	0.6465	−2.4697	−1.8039
3	−0.8428	−2.8094	−0.2500	−0.9806
4	2.1356	−6.4652	−0.6517	−0.8255
Delta	6.5539	9.3970	2.2198	1.2607
Rank	2	1	3	4

*Smaller is better

Table 8 Response table for S/N ratios of wear resistance

Level	Plate/pin type	Applied load (N)	Sliding velocity (m/s)	Sliding distance (m)
1	−4.3837	2.9708	−2.2967	−2.0235
2	−2.5145	0.6768	−2.4221	−1.7714
3	−0.8017	−2.7877	−0.2132	−0.9546
4	2.1443	−6.4154	−0.6235	−0.8060
Delta	6.5280	9.3862	2.2089	1.2175
Rank	2	1	3	4

*Larger is better

Table 9 Response table for S/N ratios of COF

Level	Plate/pin type	Applied load (N)	Sliding velocity (m/s)	Sliding distance (m)
1	−11.107	−9.656	−9.652	−11.708
2	−8.800	−9.581	−9.225	−10.155
3	−9.726	−9.055	−8.985	−8.495
4	−7.991	−9.333	−9.762	−7.266
Delta	3.116	0.601	0.777	4.442
Rank	2	4	3	1

*Larger is better

of anti-frictional behaviour and high fracture toughness property of h-BN which is surrounded by an area with a high dislocation density. Wear resistance is improved by the interaction between h-BN and the dislocation site [28].

Confirmation Test

The optimal configurations from the findings are a composite pin, 10 N of load, 1 m/s of sliding velocity, and a 2000 m sliding distance. According to the regression equation, the GRG at the optimal parameter levels is predicted as 0.845 and the experimental GRG was found to be 0.839.

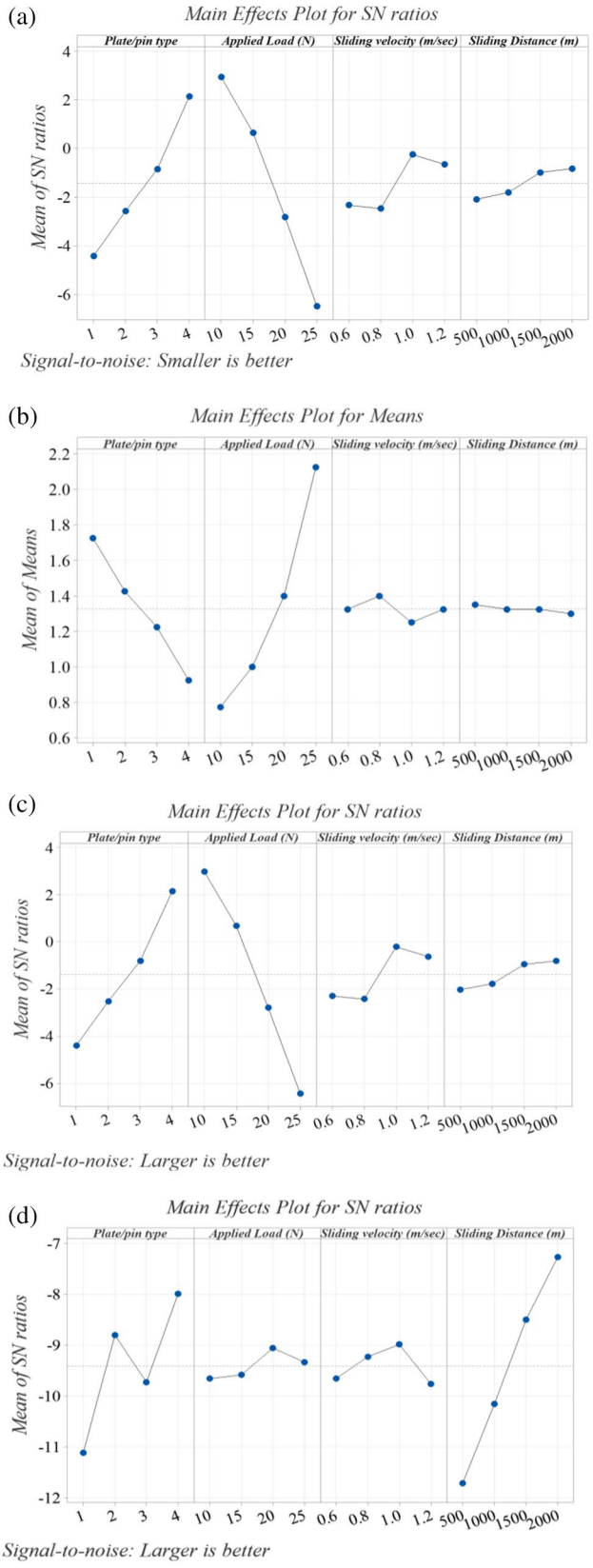

Fig. 7 Response of wear rate; **a** S/N ratios, **b** means, **c** response of wear resistance, and **d** Response of COF

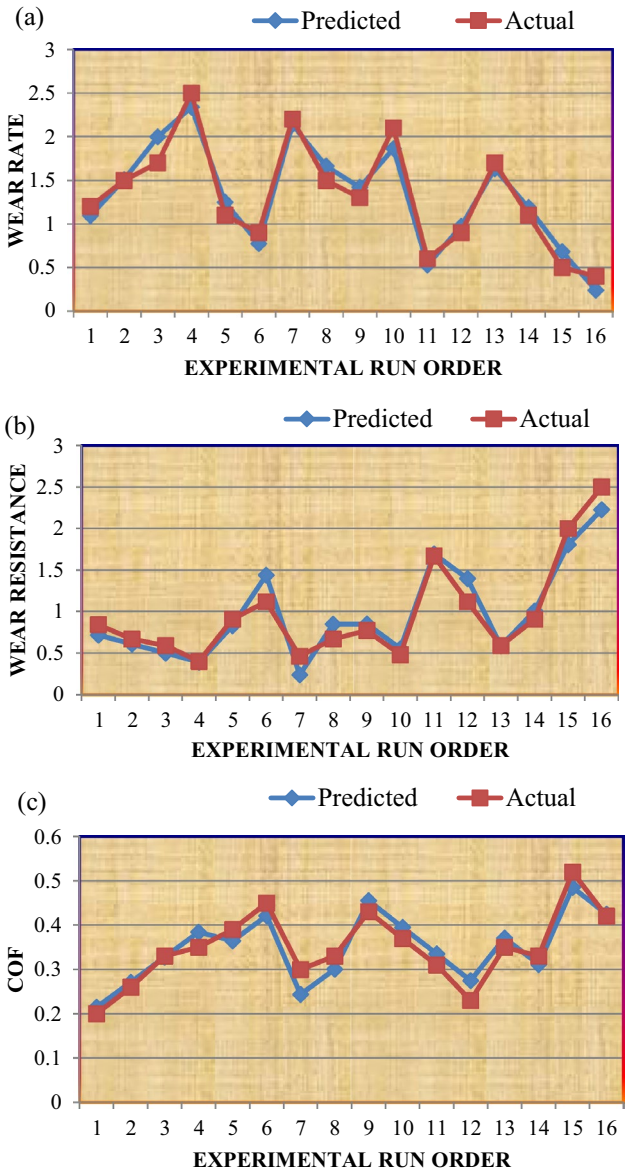

Fig. 8 Predicted versus actual; **a** wear rate, **b** wear resistance, and **c** COF

Figure 11 indicates the predicted and experimental GRG values. The determined percentage of error between the outcomes is 0.709%, which adequately demonstrates the generated model's accuracy level.

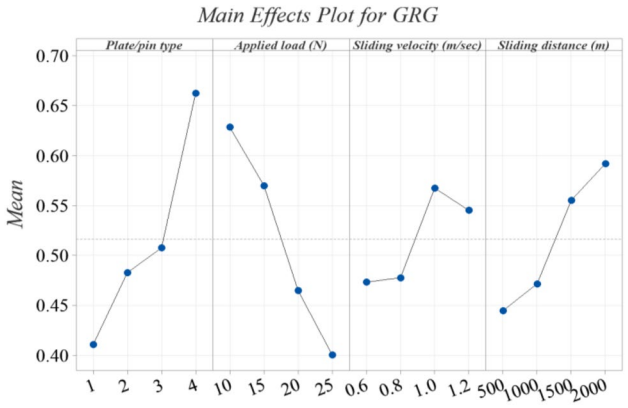

Fig. 9 Response of GRG

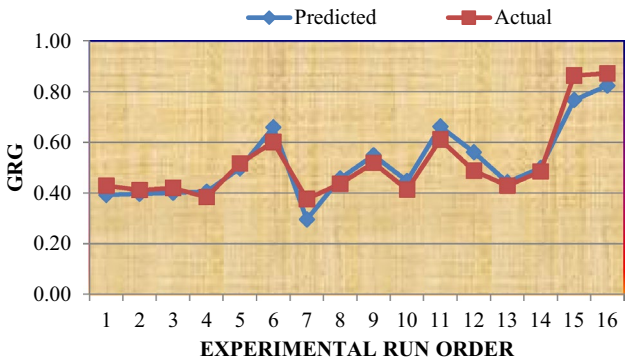

Fig. 10 Predicted versus actual GRG

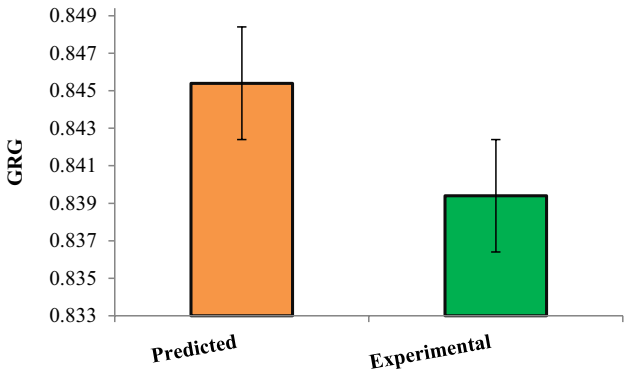

Fig. 11 Predicted and experimental GRG

Table 10 Grey relational analysis table

Runs	Normalizing sequence			Deviation sequence			Grey relational coefficient			Grey relational grade
	Wear rate	Wear resistance	COF	Wear rate	Wear resistance	COF	Wear rate	Wear resistance	COF	
1	0.619	0.210	0.000	0.381	0.790	1.000	0.568	0.387	0.333	0.429
2	0.476	0.129	0.188	0.524	0.871	0.813	0.488	0.365	0.381	0.411
3	0.381	0.090	0.406	0.619	0.910	0.594	0.447	0.355	0.457	0.420
4	0.000	0.000	0.469	1.000	1.000	0.531	0.333	0.333	0.485	0.384
5	0.667	0.243	0.594	0.333	0.757	0.406	0.600	0.398	0.552	0.516
6	0.762	0.343	0.781	0.238	0.657	0.219	0.677	0.432	0.696	0.602
7	0.143	0.029	0.313	0.857	0.971	0.688	0.368	0.340	0.421	0.376
8	0.476	0.129	0.406	0.524	0.871	0.594	0.488	0.365	0.457	0.437
9	0.571	0.176	0.719	0.429	0.824	0.281	0.538	0.378	0.640	0.519
10	0.190	0.038	0.531	0.810	0.962	0.469	0.382	0.342	0.516	0.413
11	0.905	0.605	0.344	0.095	0.395	0.656	0.840	0.559	0.432	0.610
12	0.762	0.343	0.094	0.238	0.657	0.906	0.677	0.432	0.356	0.488
13	0.381	0.090	0.469	0.619	0.910	0.531	0.447	0.355	0.485	0.429
14	0.667	0.243	0.406	0.333	0.757	0.594	0.600	0.398	0.457	0.485
15	0.952	0.762	1.000	0.048	0.238	0.000	0.913	0.677	1.000	0.863
16	1.000	1.000	0.688	0.000	0.000	0.313	1.000	1.000	0.615	0.872

Table 11 ANOVA table for GRG

Source	DF	Adj SS	Adj MS	*F* value	*P* value	% contribution
Plate/pin type	3	0.134311	0.044770	13.52	0.030	38
Applied load (N)	3	0.125771	0.041924	12.66	0.033	35
Sliding velocity (m/s)	3	0.027092	0.009031	2.73	0.216	8
Sliding distance (m)	3	0.057345	0.019115	5.77	0.092	16
Error	3	0.009933	0.003311			
Total	15	0.354453				

Table 12 Response table for Means of GRG

Level	Plate/pin type	Applied Load (N)	Sliding velocity (m/ss)	Sliding distance (m)
1	0.4110	0.6283	0.4734	0.4448
2	0.4828	0.5699	0.4778	0.4718
3	0.5077	0.4650	0.5674	0.5553
4	0.6623	0.4006	0.5452	0.5919
Delta	0.2512	0.2277	0.0941	0.1471
Rank	1	2	4	3

*Larger is better

Conclusions

The fabrication of reinforced and unreinforced weld through two pass FSW was accomplished. Wear study on Parent alloys, unreinforced and reinforced was carried out based on Taguchi (L_{16}) orthogonal array. The summarized conclusions of the findings are as follows:

1. The regression models generated were effectively used to predict wear rate, wear resistance, and COF. The optimal conditions for the wear responses were obtained using S/N ratios and ANOVA.
2. Normal probability distribution, residual graphs, interaction, and contour plots representing the wear responses have been interpreted to study the wear behaviour of parent and welded joints. A state of coherency exists between the optimal conditions arrived using Individual response optimization and the GRA technique.
3. For overall wear output responses, the combination of a composite pin, 10 N, 1.0 m/s, and 2000 m is identified as optimal conditions due to effective dynamic surface interaction, interfacial lubrication, and efficacious bonding between reinforcement and the weld matrix.

4. The difference in error rate (0.709%) between observed and predicted outcomes demonstrates a level of accuracy of the generated regression model.
5. The h-BN reinforced composite pin exhibits promising tribological characteristics feasible for aerospace and automobile sectors.

Funding The author(s) have received no financial support for the research, authorship, and/or publication of this article.

Declarations

Conflict of interest The author declares no conflict of interest with respect to the research, authorship, and/or publication of this article.

References

1. A. Singh, V. Upadhyay, Mechanical and microstructural behavior of similar and dissimilar AA6082-T6 and AA7050-T7 friction stir welded joints. J. Inst. Eng. India Ser. D **6**, 66 (2022)
2. D. Surrya Prakash, N. Dilip Raja, Investigation of tribological behavior on the mechanical properties of TiB_2, Al_2O_3 reinforced AA6061 matrix sintered hybrid composites. Iran. J. Mater. Sci. Eng. **18**(4), 1–13 (2021)
3. M. Paidpilli, K. Verma, R. Pandey, A. Upadhyaya, Influence of mechanical alloying and lead content on microstructure, hardness and tribological behavior of 6061 aluminium alloys. Iran. J. Mater. Sci. Eng. **14**(1), 12–23 (2017)
4. G. Naveen Kumar, R. Narayanasamy, S. Natarajan, S.P. Kumaresh Babu, K. Sivaprasad, S. Sivasankaran, Dry sliding wear behaviour of AA 6351-ZrB_2 in situ composite at room temperature. Mater. Des. **31**(3), 1526–1532 (2010)
5. G. Kasirajan, R. Rengarajan Sathish, G.R. Ashok Kumar, V.S. Raghav, K.J. Nagarajan. Rao, Tensile and wear behaviour of friction stir welded AA5052 and AA6101-T6 aluminium alloys: effect of welding parameters. Metall. Res. Technol. **117**(4), 405 (2020)
6. R. Ashok Kumar, R. Muneeswaran, M. Saravana Mohan, S. Rengarajan, G.R. Raghav, K.J. Nagarajan, Effects of tool pin profile on tensile and wear behaviour of friction stir welded AA6101-T6 and AA1350 alloys. Metall. Res. Technol. **117**, 503 (2020)
7. C. Kannan, R. Ramanujam, A.S.S. Balan, Mathematical modeling and optimization of tribological behaviour of Al 7075 based hybrid nanocomposites. P. I. Mech. Eng. J-J. Eng. **66**, 1–14 (2020)
8. P. Samal, P.R. Vundavilli, A. Meher, M.M. Mahapatra, Multi-response modeling for sliding wear behavior of AA5052/TiC composites by stir casting: a comparative analysis using response surface methodology and fuzzy logic system. P. I. Mech. Eng. E J. Pro. **66**, 1–13 (2021)
9. I. Dinaharan, R. Palanivel, N. Murugan, R.F. Laubscher, Application of artificial neural network in predicting the wear rate of copper surface composites produced using friction stir processing. Aust. J. Mech. Eng. **66**, 1–12 (2020)
10. O. Ikumapayi, E. Akinlabi, A. Sharma, V. Sharma, O. Oladijo, Tribological, structural and mechanical characteristics of friction stir processed aluminium-based matrix composites reinforced with stainless steel micro-particles. Eng. Solid Mech. **8**(3), 253–270 (2020)
11. R.B. Naik, G.M. Reddy, S.K. Subbu, R.A. Kumar, Optimization of friction stir processing parameters for the development of Cu–W surface composite. Mater. Sci. Forum. **969**, 864–869 (2019)
12. G. Girish, V. Anandakrishnan, Optimization of dry sliding wear parameters of recursive friction stir processed aluminium 7075 alloy. P. I. Mech. Eng. J-J. Eng. **66**, 1–10 (2020)
13. A.A. Adediran, K.K. Alaneme, I.O. Oladele, E.T. Akinlabi, Wear characteristics of aluminium matrix composites reinforced with Si-based refractory compounds derived from rice husks. Cogent Eng. **7**(1), 1826634 (2020)
14. A. Saravanakumar, L. Rajeshkumar, D. Balaji, M.P.J. Karunan, Prediction of wear characteristics of AA2219-Gr matrix composites using GRNN and Taguchi-based approach. Arab. J. Sci. Eng. **6**, 66 (2020)
15. Q. Zhao, Y. Liang, Z. Zhang, X. Li, L. Ren, Microstructure and Dry-Sliding Wear Behavior of B_4C Ceramic Particulate Reinforced Al 5083 Matrix Composite. Metals. **6**(9), 227 (2016)
16. A. Coyal, N. Yuvaraj, R. Butola, L. Tyagi, An experimental analysis of tensile, hardness and wear properties of aluminium metal matrix composite through stir casting process. SN Appl. Sci. **2**(5), 66 (2020)
17. O.C. Mata, A.F.M. Perez, G.Y.P. Medina, F.J.G. Vazquez, A. Arizmendi, Wear resistance analysis of A359/SiC/20p advanced composite joints welded by friction stir welding. Soldag. Insp. **21**(2), 220–227 (2016)
18. M. Madhusudan, S.P. Shanmuganatan, K. Shridhar, J. John, R. Krishnamurthy, B. Sasikumar, Investigation on friction stir weldability characteristics of AA7075-T651 and AA6061-T6 based nanocomposites. Adv. Mater. Sci. Eng. **66**, 3536353 (2021)
19. ASTM G99 Standard Guide for Preparation of Wear test Specimens
20. K. Ragupathy, C. Velmurugan, N. Senthilkumar, Tribological and heat treatment prediction of stir cast Al 6061/SiC/MoS_2 composites using grey relational analysis. J. Balk. Tribol. Assoc. **24**(2), 198–217 (2018)
21. A. Baradeswaran, S.C. Vettivel, A. Elaya Perumal, N. Selvakumar, R. Franklin Issac, Experimental investigation on mechanical behaviour, modelling and optimization of wear parameters of B_4C and graphite reinforced aluminium hybrid composites. Mater. Des. **63**, 620–632 (2014)
22. S. Natarajan, R. Narayanasamy, S.P. Kumaresh Babu, G. Dinesh, B. Anil Kumar, K. Sivaprasad, Sliding wear behaviour of Al 6063/TiB_2 in situ composites at elevated temperatures. Mater. Des. **30**(7), 2521–2531 (2009)
23. B. Zahmatkesh, M.H. Enayati, F. Karimzadeh, Tribological and microstructural evaluation of friction stir processed Al2024 alloy. Mater. Des. **31**(10), 4891–4896 (2010)
24. M. Bahrami, M. Nikoo, G. Besharati, K. Mohammad, Microstructural and mechanical behaviors of nano-SiC reinforced AA7075-O FSW joints prepared through two passes. Mater. Sci. Eng. A **626**, 220–228 (2014)
25. P.P. Ikubanni, M. Oki, A.A. Adeleke, O.O. Agboola, Optimization of the tribological properties of hybrid reinforced aluminium matrix composites using Taguchi and Grey's relational analysis. Sci. Afr. **12**, 66 (2021)
26. M. Kamaraj, R. Manimaran, S. Datta, Optimization of dry sliding wear parameters of graphene-filled flax fiber-reinforced epoxy composites using Taguchi grey relational analysis. J. Inst. Eng. India Ser. D **6**, 66 (2022)
27. M. Sivanesh Prabhu, A. Elaya Perumal, S. Arulvel, R. Franklin Issac, Friction and wear measurements of friction stir processed aluminium alloy 6082/$CaCO_3$ composite. Measurement **142**, 10–20 (2019)

28. K. Kalaiselvan, N. Murugan, Dry sliding wear behaviour of friction stir welded aluminum (6061)-B_4C composite. Int. J. Microstruct. Mater. **8**(3), 239 (2013)